FULL-ENERGY PEAK EFFICIENCY OF ASYMMETRICAL POLYHEDRON GERMANIUM DETECTOR

by

Mahmoud I. ABBAS [1*], ***Sara YOSEPH*** [1], ***Ahmed M. EL-KHATIB*** [1], ***Mohamed S. BADAWI*** [1,2], ***Mona M. GOUDA*** [1], ***and Abouzeid A. THABET*** [3]

[1] Physics Department, Faculty of Science, Alexandria University, Alexandria, Egypt
[2] Department of Physics, Faculty of Science, Beirut Arab University, Beirut, Lebanon
[3] Department of Medical Equipment Technology, Faculty of Allied Medical Science, Pharos University in Alexandria, Alexandria, Egypt

Scientific paper
http://doi.org/10.2298/NTRP1802150A

To understand the nuclear structure for most elements, it is essential to investigate the nuclear excitations by using high precision gamma-ray spectroscopy in which intensive measurements should be carried out. This is becoming a new challenge for the radiation scientific community nowadays, where the instrumentations and technical advances must be developed to be used in a wide range of applications. To discover the weakest nuclear reaction, the maximum probability of the detection system of the total energy of any released individual photon must be determined. In this work, a new mathematical method to calculate the absolute full-energy peak efficiency of asymmetrical polyhedron germanium detector is presented. This type of detector can be arranged in array, forming "complex detectors of encapsulated germanium crystals", with the solid angle reaching 82 % of total solid angle coverage, *i. e.*, with the highest possible efficiency and with a good quality of spectral response. In addition, the photon path length was enclosed in the mathematical method to determine its attenuation through different materials such as, the detector active medium and any other material in-between source-detector system during the measuring process. The comparison between the efficiency calculated in this work and that of the published Monte Carlo simulation showed a good agreement and a small variation. However, the method discussed in the current work can be useful in nuclear safeguards, in overcoming the huge difficulties in identification of the energy range of radioactive isotopes and their quantities in nuclear waste.

Key words: polyhedron detector, full-energy peak efficiency, gamma-ray

INTRODUCTION

Nowadays, knowing and understanding the different nuclear excitations processes is one of the most important goals of nuclear formation theory. The most significant apparatus to examine nuclear configuration is high accuracy γ-ray spectrometers in good arrangement. Future challenges for nuclear spectroscopy are coming along with the next generation of high-intensity radioactive ion beam facilities currently being developed worldwide. A new generation of γ-spectrometers will be the Advanced Gamma Tracking Array AGATA [1, 2] in Europe and the GRETA array in the U. S. [3, 4]. These facilities will make it possible to study very short lived exotic nuclei with extreme values of isospin, located in the *terra incognita* far from the line of β stability.

The possible configurations for 4π array detector were evaluated through detailed Monte Carlo simulations of the full array [5]. The simulation code for 4 detector is based on the C++ classes of GEANT4 [5], which simulates the interaction of γ-rays in the detectors and allows the inclusion of realistic shapes and passive materials [6, 7]. One of these configurations is A180 configuration which consists of 180 asymmetric hexagonal-shaped, tapered, encapsulated HPGe detectors. Three slightly different asymmetric detectors (Red, Blue and Green detector) are combined into a triple cluster cryostats unit (60 identical cryostats). The detector configuration allows a 0.09 m thick germanium shell with up to 82 % of solid angle coverage [8].

The recent work established a new mathematical method to determine the absolute full-energy peak efficiency of asymmetric polygon germanium detector. The core of this mathematical method is based on the approach which was given earlier in [9-22], where the

* Corresponding author; e-mail: mabbas@physicist.net

integrals and its limitations became more complex and hard to obtain related to the complex source-to-detector geometry. Showing the accuracy of the present method and how it is valid in calculating the efficiency of γ-ray detector was done by comparing the results with the published Monte Carlo simulations data [23].

Mathematical view point

The validity of the present work is presented by comparing the obtained results with the published Monte Carlo simulation [23]. The full-energy peak efficiency for an axial radiating point source placed at any distance from the polyhedron design detector can be represented by the following equation based on [18]

$$\varepsilon_{ph}^{ab} \quad \frac{1}{4\pi} \int_{\varphi\,\theta} f_{\text{att}} (1 \quad e^{-\mu_p d}) \sin(\theta) \, d\theta \, d\varphi \qquad (1)$$

where θ and φ are the polar and azimuthal angles, respectively. μ_p is the peak attenuation coefficient of the detector's active medium, which represents the part contributing to the photopeak only. It is given by $\mu_p \quad \tau \quad f_m\sigma \quad g_n\kappa_{no}$ where, $\tau \quad \sigma$ and κ_{no} are the photoelectric, incoherent (Compton) and pair production (in the nuclear field) coefficients corresponding to the energy of the incident photon E_γ, respectively, the factors f_m and g_n give the fractions of the incoherent and pair production leading to the photopeak, respectively [24]. The effective rays passing through the detector crystal active volume traverse a distance d until it emerges from the detector crystal. The factor fatt determining the photon attenuation by the source container and the detector housing materials, and is expressed as

$$f_{\text{att}} \quad \prod_{q\ 1}^{Q} e^{-\mu_q \delta_q} \qquad (2)$$

where μ_q is the coefficient of attenuation per unit length of the q^{th} absorber for gamma-ray energy E_γ, δ_q is the distance traveled in the material of the q_{th} absorber, and Q denotes the number of absorbers between the source and the crystal active material. The full-energy peak efficiency for 4 asymmetric array detectors ε_t is given by,

$$\varepsilon_t \quad 60 \sum_{i\ 0}^{2} \varepsilon_i \big|_{R_{i,j}\ \text{cylinder radius}} \qquad (3)$$

where ε_i is the full energy peak efficiency of i^{th} crystal ($i = 0$ for red, $i = 1$ for blue and $i = 2$ for green). To find out ε_i we consider a polyhedron crystal intersected by a cylinder of radius Rc = 0.04 m and length = 0.09 m with a back hole of radius r_h = 0.005 m at length = = 0.013 m, as shown in figs. 1 and 2, where R_{ij} is the variable-radii of the i^{th} crystal between two j^{th} and $(j + + 1)^{\text{th}}$ successive vertices (j is the vertex number and takes values from 0 to 5) along L depth which is restricted to have values less than or equal to the cylinder radius due to the intersection.

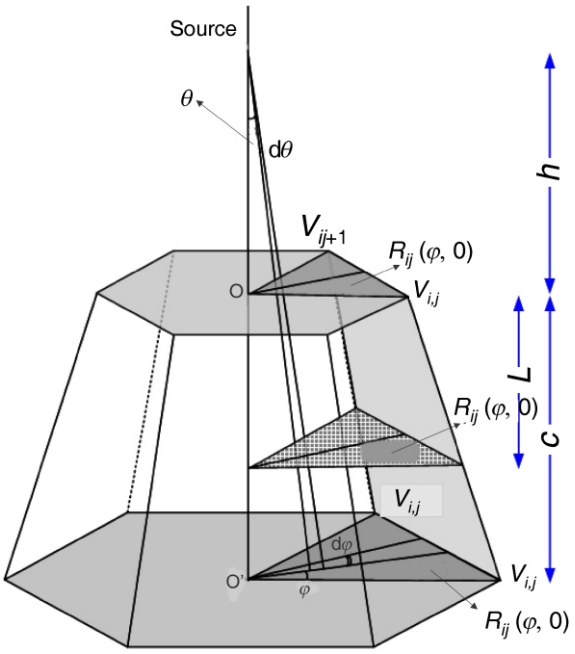

Figure 1. The polar angle θ, azimuthal angle φ and the variable radius $R_{i,j}$ (φ L) for the i^{th} crystal between V_j and V_{j+1} vertices

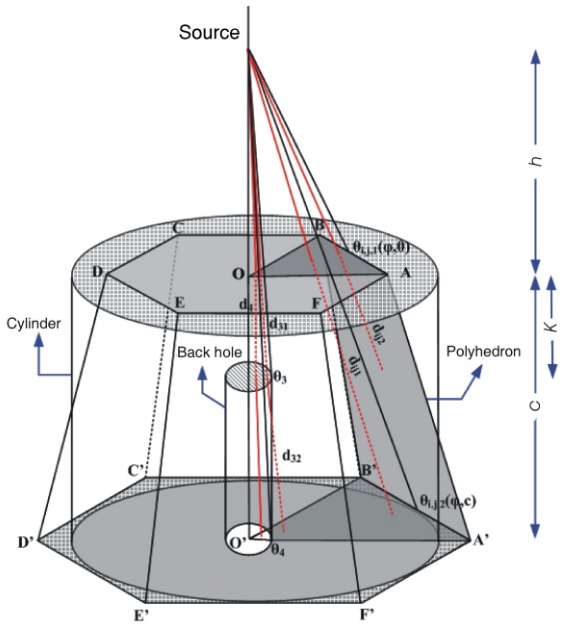

Figure 2. The polyhedron crystal intersected by a cylinder with a back hole. The schematic view of the four possible path lengths through the active volume of the crystal for the limit of the polar angle $\theta_{i,j,1}(\varphi \ \ 0) > \theta_{i,j,2}(\varphi \ \ 0) > \theta_3 > \theta_4$, irradiated by photons of point source

The polar angle θ between the two faces at depth L and azimuthal angle change according to this equation, as shown in fig. 1

$$\theta_{i,j}(\varphi, L) \quad \tan^{-1} \frac{R_{i,j}(\varphi, L)}{h \quad L} \qquad (4)$$

where L takes values from 0 to c.

It is found that there are two probabilities for the photon path lengths d traveled throughout the crystal active volume according the source-inner face distance, h, which has been obtained by solving this equation $\theta_{i,j,1}(\varphi,0)$ $\theta_{i,j,2}(\varphi,c)$, where $\theta_{i,j,1}(\varphi,0)$ is the maximum polar angle for photons to enter the detector from its upper surface and $\theta_{i,j,2}(\varphi,c)$ is the maximum polar angle for photons to leave the detector from its bottom

$$h \quad \frac{c.R_{i,j}(\varphi,0)}{R_{i,j}(\varphi,c) \quad R_{i,j}(\varphi,0)} \tag{5}$$

Then we have two different formulas for the full-energy peak efficiency for each crystal between two successive vertices j^{th} and $(j+1)^{th}$ along L depth according to the source-inner face distance.

Case a: $h \quad \frac{c.R_{i,j}(\varphi,0)}{R_{i,j}(\varphi,c) \quad R_{i,j}(\varphi,0)}$ for $\theta_{i,j,1}(\varphi,0) \quad \theta_{i,j,2}(\varphi,c)$

Case b: $h \quad \frac{c.R_{i,j}(\varphi,0)}{R_{i,j}(\varphi,c) \quad R_{i,j}(\varphi,0)}$ for $\theta_{i,j,1}(\varphi,0) \quad \theta_{i,j,2}(\varphi,c)$

As shown in figs. 2 and 3 there are four probabilities that should be considered for the photon path lengths d that traveled throughout the crystal active volume:

– The effective rays may enter the inner face of the crystal and emerge from the outer face of the crystal between polar angles θ_3 and $\theta_{i,j,2}$ (φ c in case *a*, and between polar angles θ_3 and $\theta_{i,j,1}$ (φ in case *b*

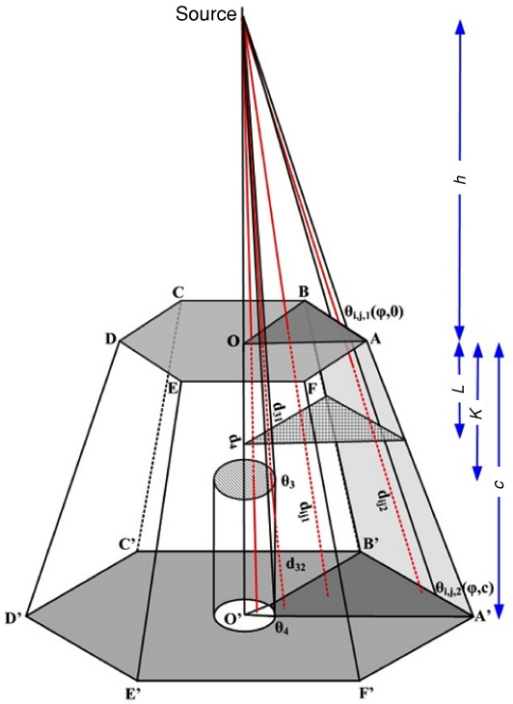

Figure 3. Schematic view of the four possible path lengths through the active volume of the crystal for the limit of the polar angle ($\theta_{i,j,2}(\varphi$ c) > $\theta_{i,j,1}$ (φ 0) > $\theta_3 > \theta_4$,), irradiated by photons of point source

$$d_{i,j,1}(\theta,\varphi,c) \quad \frac{c}{\cos[\theta(\varphi,c)]} \tag{6}$$

– The effective rays may enter the inner face of the crystal and emerge from the crystal lateral face, between polar angles $\theta_{i,j,2}$ (φ c and $\theta_{i,j,1}$ (φ 0 in case a

$$d_{i,j,2}(\theta,\varphi,L) \quad \frac{R_{i,j}(\varphi,L)}{\sin[\theta(\varphi,L)]} \quad \frac{h}{\cos[\theta(\varphi,L)]} \tag{7}$$

– or the effective rays may enter the crystal lateral face and emerge from the outer face of the crystal between polar angles $\theta_{i,j,1}$(φ and $\theta_{i,j,2}$(φ c in case *b*

$$d_{i,j,2}(\theta,\varphi,L) \quad \frac{h \quad c}{\cos[\theta(\varphi,L)]} \quad \frac{R_{i,j}(\varphi,L)}{\sin[\theta(\varphi,L)]} \tag{8}$$

– The effective rays may enter from the face of the crystal and emerge from the face of the hole then continue to enter from the hole side and emerge from the bottom of the crystal between polar angles θ_4 and θ_3 in two cases

$$d_{31}(\theta) \quad d_{32}(\theta) \quad \frac{K}{\cos(\theta)} \quad \frac{h \quad c}{\cos(\theta)} \quad \frac{r_h}{\sin(\theta)} \tag{9}$$

– Enters from the face of the crystal and emerges from face of the hole between polar angles 0 and in two cases

$$d_4(\theta) \quad \frac{K}{\cos(\theta)} \tag{10}$$

The polar angles θ_3 and θ_4 take the following corresponding values

$$\theta_3 \quad \tan^{1}\frac{r_h}{h \quad K} \tag{11}$$

$$\theta_4 \quad \tan^{1}\frac{r_h}{h \quad c} \tag{12}$$

where $\theta_4 < \theta_3$.

The full-energy peak efficiency for the i^{th} crystal is given by

$$\varepsilon_i \quad \frac{1}{4\pi} \quad 2\int_0^{\pi}\int_0^{\theta_4} f_4(\theta)\mathrm{d}\theta\mathrm{d}\varphi \int_{\theta_4}^{\theta_3} f_3(\theta)\mathrm{d}\theta\mathrm{d}\varphi \quad \sum_{j\ 0}^{5}\varepsilon_{ij} \tag{13}$$

where $J[\theta_{i,j}(\varphi \quad L), L$ is the Jacobian of $\theta_{i,j}(\varphi \quad L)$, with respect to L, and

$$f_3(\theta) \quad f_{\text{att}}(1 \quad \mathrm{e}^{\ \mu[d_{31}(\theta) \quad d_{32}(\theta)]})\sin(\theta) \tag{14}$$

$$f_4(\theta) \quad f_{\text{att}}(1 \quad \mathrm{e}^{\ \mu d_4(\theta)})\sin(\theta) \tag{15}$$

where ε_{ij} is full-energy peak efficiency for i^{th} crystal between two successive vertices j^{th} and $(j+1)^{th}$ ($j=0$ to 5) along L depth, for case a, it is given by

$$\varepsilon_{ij} \quad \frac{1}{4\pi} \int_{\varphi \ \varphi_{ij}(c)}^{\varphi \ \varphi_{i,j\ 1}(c)}\int_{\theta_3}^{\theta_{i,j,2}(\varphi,c)} f_{i,j,1}(\theta,\varphi,c)\mathrm{d}\theta\mathrm{d}\varphi + \lim_{N} \sum_{k\ 0}^{N} \int_{\varphi \ \varphi_{i,j}(L_k)}^{\varphi \ \varphi_{i,j\ 1}(L_k)}\int_{L_k}^{L_{k\ 1}} f_{i,j,2}[\theta_{i,j}(\varphi,L),\varphi,L]\mathrm{d}\theta_{i,j}(\varphi,L)\mathrm{d}\varphi \tag{16}$$

where $L_0 = c$ and $L_{N+1} = 0$

Table 1. The azimuthal angle $\varphi_{i,j}(L)$ as a function of *x*-co-ordinate $x_{i,j}(L)$ and *y*-co-ordinate $y_{i,j}(L)$ at length L from the inner face of each polyhedron crystal for each lateral edge, where $x_{i,j,a}$, $x_{i,j,b}$, $y_{i,j,a}$ and $y_{i,j,b}$ are the *x* and *y*-co-ordinates of inner and outer face of i^{th} crystal and j^{th} vertex

$x_{i,j}(L)$	$y_{i,j}(L)$	$\varphi_{i,j}(L)$
$x_{00}(L) = x_{00a} + (x_{00b} - x_{00a})\,L/c$	$y_{00}(L) = y_{00b}\,L/c$	$\varphi_{00}(L) = 2\pi - \tan^{-1}\left\|\frac{y_{00}(L)}{x_{00}(L)}\right\|$
$x_{01}(L) = x_{01a} + (x_{01b} - x_{01a})\,L/c$	$y_{01}(L) = y_{01a} + (y_{01b} - y_{01a})\,L/c$	$\varphi_{01}(L) = \tan^{-1}\left\|\frac{y_{01}(L)}{x_{01}(L)}\right\|$
$x_{02}(L) = x_{02a} + (x_{02b} - x_{02a})\,L/c$	$y_{02}(L) = y_{02a} + (y_{02b} - y_{02a})\,L/c$	$\varphi_{02}(L) = \tan^{-1}\left\|\frac{y_{02}(L)}{x_{02}(L)}\right\|$
$x_{03}(L) = x_{03a} + (x_{03b} - x_{03a})\,L/c$	$y_{03}(L) = y_{03a} + (y_{03b} - y_{03a})\,L/c$	$\varphi_{03}(L) = \pi + \tan^{-1}\left\|\frac{y_{03}(L)}{x_{03}(L)}\right\|$
$x_{04}(L) = x_{04a} + (x_{04b} - x_{04a})\,L/c$	$y_{04}(L) = y_{04a} + (y_{04b} - y_{04a})\,L/c$	$\varphi_{04}(L) = \pi + \tan^{-1}\left\|\frac{y_{04}(L)}{x_{04}(L)}\right\|$
$x_{05}(L) = x_{05a} + (x_{05b} - x_{05a})\,L/c$	$y_{05}(L) = y_{05a} + (y_{05b} - y_{05a})\,L/c$	$\varphi_{05}(L) = 2\pi - \tan^{-1}\left\|\frac{y_{05}(L)}{x_{05}(L)}\right\|$
$x_{10}(L) = x_{10a} + (x_{10b} - x_{10a})\,L/c$	$y_{10}(L) = y_{10a} + (y_{10b} - y_{10a})\,L/c$	$\varphi_{10}(L) = \tan^{-1}\left\|\frac{y_{10}(L)}{x_{10}(L)}\right\|$
$x_{11}(L) = x_{11a} + (x_{11b} - x_{11a})\,L/c$	$y_{11}(L) = y_{11a} + (y_{11b} - y_{11a})\,L/c$	$\varphi_{11}(L) = \tan^{-1}\left\|\frac{y_{11}(L)}{x_{11}(L)}\right\|$
$x_{12}(L) = x_{12a} + (x_{12b} - x_{12a})\,L/c$	$y_{12}(L) = y_{12a} + (y_{12b} - y_{12a})\,L/c$	$\varphi_{12}(L) = \pi - \tan^{-1}\left\|\frac{y_{12}(L)}{x_{12}(L)}\right\|$
$x_{13}(L) = x_{13a} + (x_{13b} - x_{13a})\,L/c$	$y_{13}(L) = y_{13a} + (y_{13b} - y_{13a})\,L/c$	$\varphi_{13}(L) = \pi - \tan^{-1}\left\|\frac{y_{13}(L)}{x_{13}(L)}\right\|$
$x_{14}(L) = x_{14a} + (x_{14b} - x_{14a})\,L/c$	$y_{14}(L) = y_{14a} + (y_{14b} - y_{14a})\,L/c$	$\varphi_{14}(L) = \pi + \tan^{-1}\left\|\frac{y_{14}(L)}{x_{14}(L)}\right\|$
$x_{15}(L) = x_{15a} + (x_{15b} - x_{15a})\,L/c$	$y_{15}(L) = y_{15a} + (y_{15b} - y_{15a})\,L/c$	$\varphi_{15}(L) = 2\pi - \tan^{-1}\left\|\frac{y_{15}(L)}{x_{15}(L)}\right\|$
$x_{20}(L) = x_{20a} + (x_{20b} - x_{20a})\,L/c$	$y_{20}(L) = y_{20a} + (y_{20} - y_{20a})\,L/c$	$\varphi_{20}(L) = 2\pi - \tan^{-1}\left\|\frac{y_{20}(L)}{x_{20}(L)}\right\|$
$x_{21}(L) = x_{21a} + (x_{21b} - x_{21a})\,L/c$	$y_{21}(L) = y_{21a} + (y_{21b} - y_{21a})\,L/c$	$\varphi_{21}(L) = \tan^{-1}\left\|\frac{y_{21}(L)}{x_{21}(L)}\right\|$
$x_{22}(L) = x_{22a} + (x_{22b} - x_{22a})\,L/c$	$y_{22}(L) = y_{22a} + (y_{22b} - y_{22a})\,L/c$	$\varphi_{22}(L) = \pi - \tan^{-1}\left\|\frac{y_{22}(L)}{x_{22}(L)}\right\|$
$x_{23}(L) = x_{23a} + (x_{23b} - x_{23a})\,L/c$	$y_{23}(L) = y_{23a} + (y_{23b} - y_{23a})\,L/c$	$\varphi_{23}(L) = \pi - \tan^{-1}\left\|\frac{y_{23}(L)}{x_{23}(L)}\right\|$
$x_{24}(L) = x_{24a} + (x_{24b} - x_{24a})\,L/c$	$y_{24}(L) = y_{24a} + (y_{24b} - y_{24a})\,L/c$	$\varphi_{24}(L) = \pi + \tan^{-1}\left\|\frac{y_{24}(L)}{x_{24}(L)}\right\|$
$x_{25}(L) = x_{25a} + (x_{25b} - x_{25a})\,L/c$	$y_{25}(L) = y_{25a} + (y_{25b} - y_{25a})\,L/c$	$\varphi_{25}(L) = 2\pi - \tan^{-1}\left\|\frac{y_{25}(L)}{x_{25}(L)}\right\|$

$$\varepsilon_{ij} \frac{1}{4\pi} \int_{\varphi=\varphi_{i,j-1}(c)}^{\varphi_{i,j,2}(\varphi,c)} \int_{\varphi=\varphi_{i,j}(c)}^{\theta_3} f_{i,j,1}(\theta,\varphi,c)\,\mathrm{d}\theta\,\mathrm{d}\varphi + \int_{0}^{\varphi_{i,j-1}(L)} \int_{c}^{\varphi=\varphi_{i,j}(L)} f_{i,j,2}[\theta_{i,j}(\varphi,L),\varphi,L]\left|J(\theta_{i,j}(\varphi,L),L)\right|\mathrm{d}\varphi\,\mathrm{d}L \quad (17)$$

for case *b*, it is given by

$$\varepsilon_{ij} \frac{1}{4\pi} \int_{\varphi=\varphi_{i,j-1}(c)}^{\varphi_{i,j,1}(\varphi,0)} \int_{\varphi=\varphi_{i,j}(c)}^{\theta_3} f_{i,j,1}(\theta,\varphi,c)\,\mathrm{d}\theta\,\mathrm{d}\varphi + \lim_{N} \sum_{k=0}^{N} \int_{\varphi=\varphi_{i,j}(L_k)}^{\varphi_{i,j-1}(L_k)} \int_{\theta_{i,j}(\varphi,L_k)}^{\theta_{i,j}(\varphi,L_{k-1})} f_{i,j,2}[\theta_{i,j}(\varphi,L),\varphi,L]\,\mathrm{d}\theta_{i,j}(\varphi,L)\mathrm{d}\varphi \quad (18)$$

where $L_0 = 0$ and $L_{N+1} = c$

Table 2. The cross-sectional variable-radius $R_{i,j}(\varphi, L)$ of the hexagonal crystal as a function of $\varphi_{i,j}(L)$ for any point lies on one of lateral faces at length L from the inner face of each polyhedron crystal for each lateral edge

$R_{i,j}(\varphi, L)$	$\delta_{i,j}(L)$	$\psi_{i,j}(L)$
$\frac{R_{00}(\varphi,L)}{\sqrt{(x_{00}(L))^2 \quad (y_{00}(L))^2 \sin(\psi_{00}(L) \quad \delta_{00}(L))}}{\sin(\varphi \quad \varphi_{00}(L) \quad \psi_{00}(L) \quad \delta_{00}(L))}$	$\delta_{00}(L) \quad \tan^{1} \frac{x_{00}(L) \quad x_{01}(L)}{\lvert y_{00}(L)\rvert \quad y_{01}(L)}$	$\psi_{00}(L) \quad \tan^{1} \frac{x_{00(L)}}{\lvert y_{00}(L)\rvert \quad 0.00001}$
$\frac{R_{01}(\varphi,L)}{\sqrt{(x_{01}(L))^2 \quad (y_{01}(L))^2 \sin(\psi_{01}(L) \quad \delta_{01}(L))}}{\sin(\varphi \quad \varphi_{01}(L) \quad \psi_{01}(L) \quad \delta_{01}(L))}$	$\delta_{01}(L) \quad \tan^{1} \frac{y_{01}(L) \quad y_{02}(L)}{x_{01}(L) \quad \lvert x_{02}(L)\rvert}$	$\psi_{01}(L) \quad \tan^{1} \frac{y_{01}(L)}{x_{01}(L)}$
$\frac{R_{02}(\varphi,L)}{\sqrt{(x_{02}(L))^2 \quad (y_{02}(L))^2 \sin(\psi_{02}(L) \quad \delta_{02}(L))}}{\sin(\varphi \quad \varphi_{02}(L) \quad \psi_{02}(L) \quad \delta_{02}(L))}$	$\delta_{02}(L) \quad \tan^{1} \frac{\lvert x_{03}(L)\rvert \quad \lvert x_{02}(L)\rvert}{y_{02}(L) \quad \lvert y_{03}(L)\rvert}$	$\psi_{02}(L) \quad \tan^{1} \left\lvert \frac{x_{02}(L)}{y_{02}(L)} \right\rvert$
$\frac{R_{03}(\varphi,L)}{\sqrt{(x_{03}(L))^2 \quad (y_{03}(L))^2 \sin(\psi_{03}(L) \quad \delta_{03}(L))}}{\sin(\psi_{03}(L) \quad \delta_{03}(L) \quad \varphi \quad \varphi_{03}(L))}$	$\delta_{03}(L) \quad \tan^{1} \frac{\lvert x_{03}(L)\rvert \quad \lvert x_{04}(L)\rvert}{\lvert y_{04}(L)\rvert \quad \lvert y_{03}(L)\rvert}$	$\psi_{03}(L) \quad \tan^{1} \left\lvert \frac{x_{03}(L)}{y_{03}(L)} \right\rvert$
$\frac{R_{04}(\varphi,L)}{\sqrt{(x_{04}(L))^2 \quad (y_{04}(L))^2 \sin(\psi_{04}(L) \quad \delta_{04}(L))}}{\sin(\varphi \quad \varphi_{04}(L) \quad \psi_{04}(L) \quad \delta_{04}(L))}$	$\delta_{04}(L) \quad \tan^{1} \frac{\lvert y_{05}(L)\rvert \quad \lvert y_{04}(L)\rvert}{x_{05}(L) \quad \lvert x_{04}(L)\rvert}$	$\psi_{04}(L) \quad \tan^{1} \left\lvert \frac{x_{04}(L)}{y_{04}(L)} \right\rvert$
$\frac{R_{05}(\varphi,L)}{\sqrt{(x_{05}(L))^2 \quad (y_{05}(L))^2 \sin(\psi_{05}(L) \quad \delta_{05}(L))}}{\sin(\varphi \quad \varphi_{05}(L) \quad \psi_{05}(L) \quad \delta_{05}(L))}$	$\delta_{05}(L) \quad \tan^{1} \frac{x_{00}(L) \quad x_{05}(L)}{\lvert y_{05}(L)\rvert \quad \lvert y_{00}(L)\rvert}$	$\psi_{05}(L) \quad \tan^{1} \left\lvert \frac{x_{05}(L)}{y_{05}(L)} \right\rvert$
$\frac{R_{10}(\varphi,L)}{\sqrt{(x_{10}(L))^2 \quad (y_{10}(L))^2 \sin(\psi_{10}(L) \quad \delta_{10}(L))}}{\sin(\varphi_{10}(L) \quad \varphi \quad \psi_{10}(L) \quad \delta_{10}(L))}$	$\delta_{10}(L) \quad \tan^{1} \frac{x_{10}(L) \quad x_{11}(L)}{y_{11}(L) \quad y_{10}(L)}$	$\psi_{10}(L) \quad \tan^{1} \frac{x_{10(L)}}{y_{10}(L) \quad 0.00001}$
$\frac{R_{11}(\varphi,L)}{\sqrt{(x_{11}(L))^2 \quad (y_{11}(L))^2 \sin(\psi_{11}(L) \quad \delta_{11}(L))}}{\sin(\varphi \quad \varphi_{11}(L) \quad \psi_{11}(L) \quad \delta_{11}(L))}$	$\delta_{11}(L) \quad \tan^{1} \frac{y_{11}(L) \quad x_{01}(L)}{x_{11}(L) \quad \lvert x_{12}(L)\rvert}$	$\psi_{11}(L) \quad \tan^{1} \frac{y_{11}(L)}{x_{11}(L)}$
$\frac{R_{12}(\varphi,L)}{\sqrt{(x_{12}(L))^2 \quad (y_{12}(L))^2 \sin(\psi_{12}(L) \quad \delta_{12}(L))}}{\sin(\varphi \quad \varphi_{12}(L) \quad \psi_{12}(L) \quad \delta_{12}(L))}$	$\delta_{12}(L) \quad \tan^{1} \frac{\lvert x_{13}(L)\rvert \quad \lvert x_{12}(L)\rvert}{y_{12}(L) \quad y_{13}(L)}$	$\psi_{12}(L) \quad \tan^{1} \left\lvert \frac{x_{12}(L)}{y_{12}(L)} \right\rvert$
$\frac{R_{13}(\varphi,L)}{\sqrt{(x_{13}(L))^2 \quad (y_{13}(L))^2 \sin(\psi_{13}(L) \quad \delta_{13}(L))}}{\sin(\varphi \quad \varphi_{13}(L) \quad \psi_{13}(L) \quad \delta_{13}(L))}$	$\delta_{13}(L) \quad \tan^{1} \frac{\lvert x_{13}(L)\rvert \quad \lvert x_{14}(L)\rvert}{\lvert y_{14}(L)\rvert \quad y_{13}(L)}$	$\psi_{13}(L) \quad \tan^{1} \frac{\lvert x_{13}(L)\rvert}{y_{13}(L)}$
$\frac{R_{14}(\varphi,L)}{\sqrt{(x_{14}(L))^2 \quad (y_{14}(L))^2 \sin(\psi_{14}(L) \quad \delta_{14}(L))}}{\sin(\varphi \quad \varphi_{14}(L) \quad \psi_{14}(L) \quad \delta_{14}(L))}$	$\delta_{14}(L) \quad \tan^{1} \frac{\lvert y_{15}(L)\rvert \quad \lvert y_{14}(L)\rvert}{x_{15}(L) \quad \lvert x_{14}(L)\rvert}$	$\psi_{14}(L) \quad \tan^{1} \left\lvert \frac{y_{14}(L)}{x_{14}(L)} \right\rvert$
$\frac{R_{15}(\varphi,L)}{\sqrt{(x_{15}(L))^2 \quad (y_{15}(L))^2 \sin(\psi_{15}(L) \quad \delta_{15}(L))}}{\sin(\varphi \quad \varphi_{15}(L) \quad \psi_{15}(L) \quad \delta_{15}(L))}$	$\delta_{15}(L) \quad \tan^{1} \frac{x_{10}(L) \quad x_{15}(L)}{\lvert y_{15}(L)\rvert \quad y_{10}(L)}$	$\psi_{15}(L) \quad \tan^{1} \frac{x_{15}(L)}{\lvert y_{15}(L)\rvert}$
$\frac{R_{20}(\varphi,L)}{\sqrt{(x_{20}(L))^2 \quad (y_{20}(L))^2 \sin(\psi_{20}(L) \quad \delta_{20}(L))}}{\sin(\varphi \quad \varphi_{20}(L) \quad \psi_{20}(L) \quad \delta_{20}(L))}$	$\delta_{20}(L) \quad \tan^{1} \frac{x_{20}(L) \quad x_{21}(L)}{\lvert y_{20}(L)\rvert \quad y_{21}(L)}$	$\psi_{20}(L) \quad \tan^{1} \frac{x_{20(L)}}{\lvert y_{20}(L)\rvert \quad 0.00001}$

Table 2. (continuation)

$R_{i,j}(\varphi, L)$	$\delta_{i,j}(L)$	$\psi_{i,j}(L)$
$\dfrac{R_{21}(\varphi,L)}{\sqrt{(x_{21}(L))^2 \quad (y_{21}(L))^2}\sin(\psi_{21}(L) \quad \delta_{21}(L))}{\sin(\varphi \quad \varphi_{21}(L) \quad \psi_{21}(L) \quad \delta_{21}(L))}$	$\delta_{21}(L) \quad \tan^{1}\dfrac{y_{21}(L) \quad y_{22}(L)}{x_{21}(L) \quad \lvert x_{22}(L)\rvert}$	$\psi_{21}(L)$ $\tan^{1}\dfrac{y_{21}(L)}{x_{21}(L)}$
$\dfrac{R_{22}(\varphi,L)}{\sqrt{(x_{22}(L))^2 \quad (y_{22}(L))^2}\sin(\psi_{22}(L) \quad \delta_{22}(L))}{\sin(\varphi \quad \varphi_{22}(L) \quad \psi_{22}(L) \quad \delta_{22}(L))}$	$\delta_{22}(L) \quad \tan^{1}\dfrac{\lvert x_{23}(L)\rvert \quad \lvert x_{22}(L)\rvert}{y_{22}(L) \quad y_{23}(L)}$	$\psi_{22}(L)$ $\tan^{1}\dfrac{\lvert x_{22}(L)\rvert}{y_{22}(L)}$
$\dfrac{R_{23}(\varphi,L)}{\sqrt{(x_{23}(L))^2 \quad (y_{23}(L))^2}\sin(\psi_{23}(L) \quad \delta_{23}(L))}{\sin(\varphi \quad \psi_{23}(L) \quad \delta_{23}(L) \quad \varphi_{23}(L))}$	$\delta_{23}(L) \quad \tan^{1}\dfrac{\lvert x_{23}(L)\rvert \quad \lvert x_{24}(L)\rvert}{\lvert y_{24}(L)\rvert \quad y_{23}(L)}$	$\psi_{23}(L)$ $\tan^{1}\dfrac{\lvert x_{23}(L)\rvert}{y_{23}(L)}$
$\dfrac{R_{24}(\varphi,L)}{\sqrt{(x_{24}(L))^2 \quad (y_{24}(L))^2}\sin(\psi_{24}(L) \quad \delta_{24}(L))}{\sin(\varphi \quad \varphi_{24}(L) \quad \psi_{024}(L) \quad \delta_{24}(L))}$	$\delta_{24}(L) \quad \tan^{1}\dfrac{\lvert x_{25}(L)\rvert \quad \lvert y_{24}(L)\rvert}{x_{25}(L) \quad \lvert x_{24}(L)\rvert}$	$\psi_{24}(L)$ $\tan^{1}\dfrac{\lvert y_{24}(L)\rvert}{x_{24}(L)}$
$\dfrac{R_{25}(\varphi,L)}{\sqrt{(x_{25}(L))^2 \quad (y_{25}(L))^2}\sin(\psi_{25}(L) \quad \delta_{25}(L))}{\sin(\varphi \quad \varphi_{25}(L) \quad \psi_{25}(L) \quad \delta_{25}(L))}$	$\delta_{25}(L) \quad \tan^{1}\dfrac{x_{20}(L) \quad x_{25}(L)}{\lvert y_{25}(L)\rvert \quad \lvert y_{20}(L)\rvert}$	$\psi_{25}(L)$ $\tan^{1}\dfrac{x_{25}(L)}{\lvert y_{25}(L)\rvert}$

$$\varepsilon_{ij} \quad \frac{1}{4\pi} \int_{\varphi \quad \varphi_{i,j}(c)}^{\varphi \quad \varphi_{i,j} \quad 1(c)} \int_{\theta_3}^{\theta_{i,j,1}(\varphi,0)} f_{i,j,1}(\theta,\varphi,c)\,\mathrm{d}\theta\,\mathrm{d}\varphi + \int_{0}^{c} \int_{\varphi \quad \varphi_{i,j}(L)}^{\varphi \quad \varphi_{i,j} \quad 1(L)} f_{i,j,2}(\theta_{i,j}(\varphi,L),\varphi,L)\left|J(\theta_{i,j}(\varphi,L),L)\right|\mathrm{d}\varphi\,\mathrm{d}L \tag{19}$$

where $J(\theta_{i,j}(\varphi \quad L), L$ is the Jacobian of $(\theta_{i,j}(\varphi \quad L)$ with respect to L, and

$$f_{i,j,1}(\theta,\varphi,c) \quad f_{\mathrm{att}}(1 \quad \mathrm{e}^{\mu \mathrm{d}_{i,j,1}(\theta,\varphi,c)})\sin(\theta) \tag{20}$$

$$f_{i,j,2}(\theta_{ij},\varphi,L) \quad f_{\mathrm{att}}(1 \quad \mathrm{e}^{\mu \mathrm{d}_{i,j,2}(\theta_{ij},\varphi,L)})\sin(\theta_{ij}) \tag{21}$$

The relation between x, y, and z coordinates (x, y, and z coordinates are given in ref. [25]) with the boundaries of the azimuthal $\varphi_{i,j}$ (L) angles, and the cross-sectional variable-radius $R_{i,j}(\varphi \quad L$ of the hexagonal crystal as a function of $\varphi_{i,j}(L)$ for any point lies on one of lateral faces at length L from the inner face of each polyhedron crystal for each lateral edge are given in tab. 1 and tab. 2.

RESULTS AND DISCUSSION

The full-energy peak (photopeak) efficiencies for A180 configuration 4 array detectors, in the energy range 100-2700 keV, have been calculated and compared with the published Monte Carlo simulations [23], as shown in fig. 4. Also, the discrepancies between the present theoretical methods with simulated results are tabulated in tab. 3. The obtained results

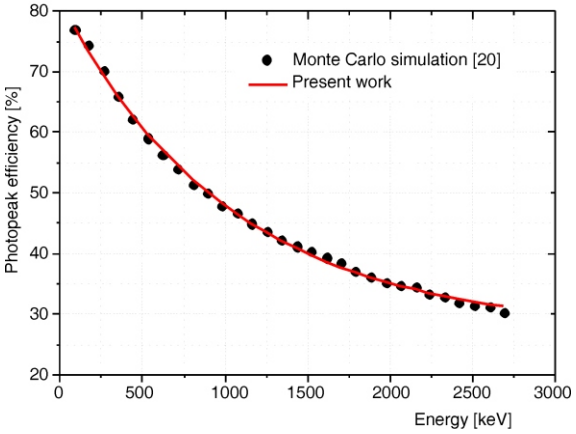

Figure 4. Comparison of Monte Carlo [23] and the present work of the full-energy peak efficiencies of 4 A180 array detector for energy range 10-2700 keV at source to inner-face distance h = 0.235 m

were found to be in a good agreement, the maximum deviation between the present theoretical methods and the published results were found to be less than 3 %.

The photopeak attenuation coefficient (cm^{-1}) at energy range 100 to 2700 keV and the fitted values using eq. (22) were presented as shown in fig. 5. The photopeak attenuation coefficient decreases rapidly at lower energies and approximately levels at high energies about 0.05 cm^{-1}. The sharp decrease in full-energy peak efficiency is reflected in the substantial change of the efficiency at low energies. The fitting equation is given by

$$\mu_{\mathrm{p}} \quad \mu_0 \quad A_1\mathrm{e}^{\frac{E}{t_1}} \quad A_2\mathrm{e}^{\frac{E}{t_2}} \tag{22}$$

Table 3. Discrepancies between Monte Carlo [23] and theoretical method results

Energy [keV]	Photopeak efficiency [%]		Discrepancies [%]
	Monte Carlo simulation [23]	Theoretical method (present work)	
87.84	77.08	77.25	0.22
168.92	74.43	73.48	–1.29
263.51	70.19	69.43	–1.10
351.35	65.96	65.99	0.05
439.19	62.25	62.83	0.92
533.78	59.07	59.71	1.08
621.62	56.42	57.06	1.14
709.46	54.02	54.63	1.11
804.05	51.37	52.23	1.65
891.89	50.03	50.18	0.31
979.73	47.90	48.31	0.85
1074.32	46.82	46.46	–0.78
1162.16	44.96	44.89	–0.16
1256.76	43.62	43.33	–0.65
1337.84	42.28	42.11	–0.40
1432.43	41.20	40.80	–0.98
1520.27	40.39	39.69	–1.76
1614.86	39.31	38.59	–1.87
1702.70	38.50	37.66	–2.24
1783.78	37.16	36.86	–0.81
1878.38	36.08	36.01	–0.20
1972.97	35.27	35.23	–0.10
2060.81	34.72	34.57	–0.43
2155.41	34.43	33.92	–1.51
2236.49	33.36	33.41	0.15
2331.08	32.81	32.86	0.16
2418.92	32.00	32.39	1.22
2506.76	31.45	31.96	1.61
2601.35	31.16	31.54	1.20
2689.19	30.35	31.18	2.67

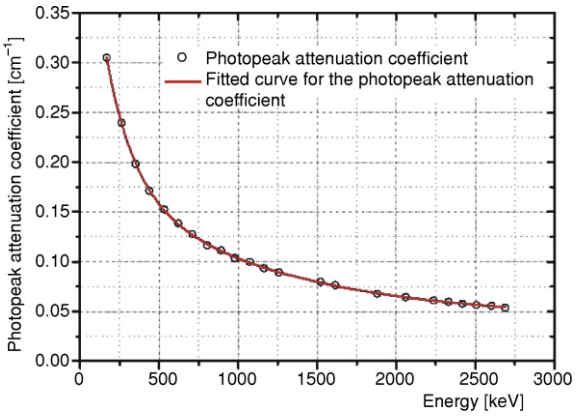

Figure 5. The photopeak attenuation coefficient (cm^{-1}) at energy range 10 to 2700 keV and its fitted values

where 0.0424 0.0004, A_1 = 0.3467 0.0032, t_1 = = 174.78 1.72, A_2 = 0.1538 0.0013, and t_2 = = 1066.28 7.21. The discrepancies between the present and fitted photopeak attenuation coefficient values are tabulated in tab. 4. The maximum deviation between the present and fitted values were found to be less than 1.1 %.

Table 4. Shows the discrepancies between present and fitted photopeak attenuation coefficient values

Energy [keV]	Photopeak attenuation coefficient [cm^{-1}]		Discrepancies [%]
	Present	Fitted value	
87.84	0.39361	0.390627714	0.76
168.92	0.30511	0.303450812	0.54
263.51	0.23965	0.237919449	0.72
351.35	0.19826	0.198502616	0.12
439.19	0.17133	0.171654433	0.19
533.78	0.15241	0.151418947	0.65
621.62	0.13874	0.137672630	0.77
709.46	0.12770	0.127026913	0.53
804.05	0.11658	0.117845488	1.09
891.89	0.11137	0.110765330	0.54
979.73	0.10355	0.104673953	1.09
1074.32	0.09979	0.098938115	0.85
1162.16	0.09356	0.094207450	0.69
1256.76	0.08929	0.089631047	0.38
1337.84	0.08600	0.086069602	0.08
1432.43	0.08220	0.082277990	0.09
1520.27	0.07960	0.079066260	0.67
1614.86	0.07656	0.075904131	0.86
1702.70	0.07310	0.073215742	0.16
1783.78	0.07070	0.070927048	0.32
1878.38	0.06790	0.068470399	0.84
1972.97	0.06610	0.066224300	0.19
2060.81	0.06442	0.064310512	0.17
2155.41	0.06220	0.062418938	0.35
2236.49	0.06106	0.060926331	0.22
2331.08	0.05972	0.059322774	0.67
2418.92	0.05779	0.057955920	0.29
2506.76	0.05650	0.056697222	0.35
2601.35	0.05580	0.055452918	0.62
2689.19	0.05395	0.054392220	0.82

CONCLUSION

In the present work, a new mathematical approach was established to calculate the absolute full-energy peak efficiency of asymmetrical polyhedron germanium detector with a closed cylindrical back hole. This approach was achieved analytically and solved numerically based on the huge amount of numbers and the difficulty of solving such integrals. This group of integrable equations include the probability to detect the total energy of any emitted photon individually for both low and high energy regions, also the effect of the source-to-detector distance, detector end cap material and the materials that were inserted and were present in the source-detector system during the measurements.

AUTHORS' CONTRIBUTIONS

The theoretical work was done by M. I. Abbas, S. Yoseph, A.M. El-Khatib, and M. S. Badawi, and all authors took part in planning the work and in discus-

sions during all phases of its elaboration. The manuscript was conceived and written by all authors. The performed data elaboration and graphical representation of results were made by all authors.

REFERENCES

[1] ***, AGATA homepage http://www.agata.org
[2] Eberth, J., Simpson, J., From Ge(Li) Detectors to Gamma-Ray Tracking Arrays – 50 Years of Gamma Spectroscopy with Germanium Detectors, *Progress in Particle and Nuclear Physics, 60* (2008), 2, pp. 283-337
[3] Deleplanque, M. A., *et al*., Accelerators, Spectrometers, Detectors and Associated Equipment, *Nuclear Instrument and Method, A430* (1999), 2-3, pp. 292-310
[4] Lee, I. Y., *et al*., Developments in Large Gamma-Ray Detector Arrays, *Reports on Progress in Physics, 66* (2003), 7, pp. 1095-1144
[5] Agostinelli, S., *et al*., Geant4 – A Simulation Toolkit, *Nuclear Instruments and Methods in Physics Research Section, A506* (2003), 3, pp. 250-303
[6] Farnea, E., *et al*., A Monte Carlo Code for the AGATA Array, LNL Annual Report 2003 LNL-INFN(REP)-202/2004, 2003
[7] Farnea, E., *et al*., Comparison of the A120, A180 Configurations, http://agata.pd.infn.it/documents/simulations/comparison.html
[8] Wiens, A., *et al*., The AGATA Triple Cluster Detector, *Nuclear Instruments and Methods in Physics Research, A618* (2010), 1-3, pp. 223-233
[9] Noureldine, S. F., *et al*., A Hybrid Analytical Numerical Method for Efficiency Calculations of Spherical Scintillation NaI(Tl) Detectors and Arbitrarily Located Point Sources, *Nucl Technol Radiat, 32* (2017), 2, pp. 140-147
[10] Gouda, M. M., *et al*., Calculation of NaI(Tl) Detector Full Energy Peak Efficiency Using the Efficiency Transfer Method for Small Radioactive Cylindrical Sources, *Nucl Technol Radiat, 31* (2016), 2, pp. 150-158
[11] Abbas, M. I., Selim, Y. S., Calculation of Relative Full-Energy Peak Efficiencies of Well-Type Detectors, *Nuclear Instruments and Methods in Physics Research, A480* (2002), 2-3, pp. 651-657
[12] Abbas, M. I., Direct Mathematical Method for Calculating Full-Energy Peak Efficiency and Coincidence Corrections of HPGe Detectors for Extended Sources, *Nuclear Instruments & Methods in Physics Research, A 256* (2007), 1, pp. 554-557
[13] Nafee, S. S., Abbas, M. I., A Theoretical Approach to Calibrate Radiation Portal Monitor (RPM) Systems, *Applied Radiation and Isotopes, 66* (2008), 10, pp. 1474-1477
[14] Nafee, S. S., Abbas, M. I., Calibration of Closed-End HPGe Detectors Using Bar (Parallelepiped) Sources, *Nuclear Instruments & Methods in Physics Research, A592* (2008), 1-2, pp. 80-87
[15] Abbas, M. I., Analytical Approach to Calculate the Efficiency of 4 NaI(Tl) Gamma-Ray Detectors for Extended Sources, *Nuclear Instruments & Methods in Physics Research, A615* (2010), 1, pp. 48-52
[16] Abbas, M. I., A New Analytical Method to Calibrate Cylindrical Phoswich and $LaBr_3$ (Ce) Scintillation Detectors, *Nuclear Instruments & Methods in Physics Research, A621* (2010), 1-3, pp. 413-418
[17] Abbas, M. I., Analytical Formulae for Borehole Scintillation Detectors Efficiency Calibration, *Nuclear Instruments & Methods in Physics Research, A622* (2010), 1, pp. 171-175
[18] Pibida, L., *et al*., Calibration of HPGe Gamma Ray Detectors for Measurement of Radioactive Noble Gas Sources, *Applied Radiation and Isotopes, 65* (2007), 2, pp. 225-233
[19] Abbas, M. I., Noureddine, S., Analytical Expression to Calculate Total and full-Energy Peak Efficiencies for cylindrical Phoswich and Lanthanum Bromide Scintillation Detectors, *Radiation Measurements, 46* (2011), 4, pp. 440-445
[20] Hamzawy, A., *et al*., New Numerical Simulation Method to Calibrate the Regular Hexagonal NaI (Tl) Detector with Radioactive Point Sources Situated Non-Axial, *Review of Scientific Instruments, 87* (2016), 11, 115105
[21] Abbas, M. I., *et al*., Analytical Formulae to Calculate the Solid Angle Subtended at an Arbitrarily Positioned Point Source by an Elliptical Radiation Detector, *Nuclear Instruments & Methods in Physics Research, A771* (2015), Jan., pp. 121-125
[22] Abbas, M. I., *et al*., Analytical Formulae to Calculate the Total Efficiency of an Arbitrarily Positioned Point Source by an Elliptical Cylindrical Detector, *Journal of Nuclear Sciences, 2* (2015), 2, pp 11-22
[23] Farnea, E., *et al*., Conceptual Design and Monte Carlo Simulations of the AGATA Array, *Nuclear Instruments and Methods in Physics Research, A621* (2010), 1-3, pp. 331-343
[24] Abbas, M. I., *et al*., Calibration of a Single Hexagonal NaI(Tl) Detector Using a New Numerical Method Based on the Efficiency Transfer Method, *Nuclear Instruments & Methods in Physics Research, A771* (2015), Jan., pp. 110-114
[25] ***, AGATA Simulation Code,http://agata.pd.infn.it/documents/simulations/agataCode.html > download the simulation code > AGATA>A180> A180solid.list

Received on November 20, 2017
Accepted on April 4, 2018

Махмуд И. АБАС, Сара ЈОСЕФ, Ахмед М. ЕЛ-КАТИБ, Мохамед С. БАДАВИ, Мона М. ГОУДА, Абузаид А. ТАБЕТ

ЕНЕРГЕТСКА ЕФИКАСНОСТ АСИМЕТРИЧНОГ ПОЛИХЕДРОНСКОГ ГЕРМАНИЈУМСКОГ ДЕТЕКТОРА

Како би се разумела структура већине елемената, потребно је испитати побуђивања језгра интензивним мерењима применом спектрометрије гама зрачења високе прецизности. Ово представља изазов научној заједници данашњице јер је потребно обезбедити инструментацију и омогућити технолошки напредак за широку примену. Да би се одредила најслабија нуклеарна реакција, мора се одредити максимална вероватноћа система детекције укупне енергије било ког ослобођеног појединачног фотона. У овом раду приказан је нови математички модел за прорачун енергетске ефикасности полихедронског германијумског детектора. Ова врста детектора може се распоредити у ред, чиме се обликује комплексни детектор око германијумског кристала са просторним углом који покрива 82 % пуног просторног угла, то јест, са највишом могућом ефикасношћу и добрим спектралним одзивом. Математички модел је обухватио и прорачун дужине путање фотона како би се одредило слабљење кроз различите материјале, као што су активна област детектора или било који други материјал који је постављен између извора и детектора током процеса мерења. Поређење израчунате ефикасности у овом раду и публикованих резултата добијених Монте Карло симулацијама показују добро слагање и малу варијацију. Штавише, приказана метода може бити употребљива у нуклеарној сигурности при савладавању потешкоћа у идентификовању енергетског опсега радиоактивних изотопа и њихове количине у радиоактивном отпаду.

Кључне речи: полихедронски детектор, ефикасност у пику енергије, гама зрачење